states histogram (see Fig. 9) which has a width at half-maximum of ~0.01 Ry or ~1.4 eV. This is narrower than the experimentally resolved structure and is in much better agreement with Eastman's work than suggested by his comparison with an extrapolated value using the zirconium results of Loucks.

V. CONCLUSIONS

The fact that little experimental data are available dictated the nature of this calculation. No attempt was made to include the spin orbit or other relativistic effects, and no effort was made to guarantee self-consistency. It is almost certainly true that some of the more subtle features of the Fermi surface will have to be modified when experimental data become available. It is hoped that this calculation will lead to an interest in the study of titanium, since it appears to be an excellent candidate for displaying all the general features exhibited by hcp metals.

ACKNOWLEDGMENTS

The authors are pleased to acknowledge the helpful comments of Larry J. Page in modifying the APW computer program for use on the Univac 1108 computer. One of us (E.H.H.) is pleased to thank Dr. Terry L. Loucks for his helpful discussion concerning the APW method and Dr. Conrad Miziumski for a stimulating discussion concerning the de Haas–van Alphen effect. A special note of thanks goes to Dr. David A. Liberman for providing the results of his atomic hfs self-consistent-field calculations for titanium which were in a form amenable to the APW method.

PHYSICAL REVIEW B VOLUME 1, NUMBER 6 15 MARCH 1970

Lattice Dynamics of Yttrium at 295 K*

S. K. SINHA, T. O. BRUN, L. D. MUHLESTEIN,† AND J. SAKURAI‡
Institute for Atomic Research and Department of Physics, Iowa State University, Ames, Iowa 50010
(Received 5 September 1969)

Phonon-dispersion curves along the [10$\bar{1}$0], [11$\bar{2}$0], and [0001] symmetry directions of the hcp metal yttrium have been measured by inelastic neutron scattering using the triple-axis neutron spectrometer at the Ames Laboratory Research Reactor. The dispersion curves are not strikingly different from those of other hcp metals with a similar c/a ratio. A careful search has been made for Kohn-type anomalies, and evidence for two such anomalies has been obtained. A modified axially symmetric force-constant model has been used to fit the phonon frequencies, and it has been found that although forces acting normally to the basal plane are not large beyond first neighbors, forces acting parallel to the basal plane are long-ranged, and interactions up to at least sixth neighbors have to be taken into account. The fitting has been done in a linear manner using Fourier analyses of the dispersion curves and other linear constraints such as the elastic constants. A frequency-distribution function has been calculated and used to calculate the specific heat and anisotropic Debye-Waller factor. Good agreement is obtained on comparison with the experimental data.

I. INTRODUCTION

OVER the last few years, neutron-scattering measurements of the phonon-dispersion curves of several hcp metals have been reported, including magnesium,[1,2] beryllium,[3,4] zinc,[5] and holmium.[6] Of these, the first three are generally regarded as free-electron–like in electronic structure. The measurements reported in this paper were originally undertaken to obtain detailed information about the lattice dynamics of the rare-earth–type metals, in view of the current interest in the properties of these metals and the considerable theoretical and experimental work being carried out in this area. Yttrium is actually to be regarded as a prototype rare-earth metal since it does not possess any f shells. However, its electronic structure[7] is very similar to the rare earths, as far as the conduction electrons are concerned, and like them it crystallizes in a hcp structure with a c/a ratio close to the ideal. The lattice constants for yttrium at room temperature are $a=3.6474$ Å, $c=5.7306$ Å, and $c/a=1.5711$. Information about the phonon spectra of the rare-earth–type metals has since been obtained by the Brookhaven group on holmium,[6] by the Oak Ridge group on holmium

* Work performed in part in the Ames Laboratory of the U. S. Atomic Energy Commission. Contribution No. 2617.
† Present address: Department of Physics, University of Missouri, Columbia, Mo. 65201.
‡ Present address: Faculty of Science, University of Hiroshima, Hiroshima, Japan.
[1] P. K. Iyengar, G. Venkataraman, P. R. Vijayaraghavan, and A. P. Roy, in *Inelastic Scattering of Neutrons in Solids and Liquids* (International Atomic Energy Agency, Vienna, 1965), Vol. I, p. 153.
[2] G. L. Squires, Proc. Phys. Soc. (London) **88**, 919 (1966); G. L. Squires and R. Pynn, in *Neutron Inelastic Scattering* (International Atomic Energy Agency, Vienna, 1968), Vol. I, p. 215.
[3] R. E. Schmunk, R. M. Brugger, P. D. Randolph, and K. A. Strong, Phys. Rev. **128**, 562 (1962).
[4] R. E. Schmunk, Phys. Rev. **149**, 450 (1966).
[5] G. Borgonovi, G. Caglioti, and J. J. Antel, Phys. Rev. **132**, 683 (1963).
[6] J. A. Leake, V. J. Minckiewicz, and G. Shirane, Solid State Commun. **7**, 535 (1969).
[7] T. L. Loucks, Phys. Rev. **144**, 504 (1966).

and terbium,[8] and by the group at Ames on scandium.[9] As expected, it turns out that all these phonon spectra look very similar, reflecting the basic similarity in conduction electron-band structures and lattice structures.

Yttrium is a very suitable candidate for an examination of the phonon problem, since, unlike the other rare-earth metals, the neutron scattering is free from all types of magnetic-scattering effects, the coherent cross section for thermal neutrons is reasonable and the neutron absorption is small. In particular, it is an obvious substance to look for effects due to the conduction electrons themselves on the phonon spectra, such as Kohn-type anomalies,[10] quite independent of effects due to the magnetic f electrons in the rare earths. Such effects have important implications in the theory of the magnetic ordering in the heavy rare-earth metals, since the well-known Ruderman-Kittel-Kasuya-Yosida (RKKY) indirect exchange interaction is there transmitted by a mechanism very similar to the ion-electron-ion interaction which determines the phonon spectra. While evidence was found of such effects in the phonon spectrum of yttrium, they were rather small as discussed below.

A rather remarkable feature of the dispersion curves is their basic similarity to those of the free-electron–like hcp metals such as magnesium and beryllium with similar c/a ratios, in spite of the rather different band structure, including considerable directional isotropy of the acoustic dispersion curves of both longitudinal and transverse polarizations. In this respect, they are rather different from the dispersion curves for zinc which has a much larger c/a ratio. Although it is in principle possible to calculate the dispersion curves for yttrium from first principles starting from the band structure,[11] it is a formidable task and we have chosen for the present to make a convenient force-constant analysis which should act essentially as an interpolation scheme for reproducing the phonon-dispersion curves. Even a Born–von Kármán analysis for the hcp structure is very complicated because of the relatively low symmetry of the structure compared to the cubic structure. Such analyses have been made for magnesium,[1,2,12–14] beryllium,[3,4,15,16] and zinc.[5,15] In order to keep their equations linear, the authors have in general restricted their number of force-constant parameters and solved for them in terms of the elastic constants and selected frequencies at symmetry points in the Brillouin zone. In general, as discussed by Raubenheimer and Gilat,[17] this results in a fit which is barely adequate along symmetry directions, and probably quite inadequate off-symmetry directions, as witnessed by the fact that the elastic constant C_{13} calculated from these models is, in general, in considerable disagreement with experiment. The most straightforward method of improving the fit is to increase the number of force constants and do a general nonlinear least-squares fit to *all* the experimental data. This method suffers from the usual defects of nonlinear least-squares fitting with a large number of adjustable parameters, namely poor convergence and no guarantee that the values obtained are unique. An alternative approach which is described in this paper is to make full use of all the linear relations obtained from both the elastic constants and a Fourier analysis of the data as described in Sec. III. In this way, one can extend the number of parameters needed to obtain a fit and yet keep the problem linear. The measured symmetry-direction branches of the dispersion curves alone do not provide enough information in principle to determine all the force constants for a general-tensor-force (GTF) model, and, hence, we have used the modified-axially symmetric (MAS) model developed by DeWames *et al.*,[15] and obtained a reasonably good fit to all the experimental data with a sixth neighbor model, although further neighbors are probably necessary for a much closer fit. We have used this model to calculate a frequency spectrum and specific heats and Debye-Waller factors for the yttrium lattice. The latter may be useful in estimating Debye-Waller factors for the rare-earth–type metals, as discussed in Sec. III, in view of the similarity in dispersion curves. This would provide more accurate Debye-Waller factors for use in interpreting the results of neutron-diffraction experiments on the rare-earth metals than has hitherto been available.

II. MEASUREMENTS

The measurements described here were carried out on a single crystal of yttrium grown from a button of crushed arc-melted yttrium metal by the method of strain annealing. The volume of the crystal was about 4 cm^3. The measurements were carried out on the Mitsubishi triple-axis spectrometer at the ALRR reactor. The incident energy was not variable for the purposes of the "constant-Q" mode of operation, but was changed between different sets of runs, for the purposes of changing the balance between intensity and resolution where required. Incident energies between 50 and 20 meV were used, the lower energies being used for high-resolution scans. Most of the scans were done using the neutron energy loss, i.e., phonon-creation process, to study the dispersion curves. The resolution function, as discussed by Cooper and Nathans,[18] was measured and used to determine the

[8] Private communication.
[9] N. Wakabayashi and S. K. Sinha, Phys. Rev. (to be published).
[10] W. Kohn, Phys. Rev. Letters **2**, 393 (1959).
[11] S. K. Sinha, Phys. Rev. **169**, 477 (1968).
[12] G. H. Begbie and M. Born, Proc. Roy. Soc. (London) **A188**, 179 (1946).
[13] L. J. Slutsky and C. S. Garland, J. Chem. Phys. **26**, 787 (1957).
[14] M. F. Collins, Proc. Phys. Soc. (London) **80**, 362 (1962).
[15] R. E. DeWames, T. Wolfram, and G. W. Lehman, Phys. Rev. **138**, A717 (1965).
[16] J. A. Young and J. U. Koppel, Phys. Rev. **134**, A1476 (1964).
[17] L. J. Raubenheimer and G. Gilat, Phys. Rev. **157**, 586 (1967).
[18] M. J. Cooper and R. Nathans, Acta Cryst. **23**, 357 (1967).

focusing conditions for the transverse phonons. Occasionally, in searching for anomalies on a longitudinal phonon branch where high resolution was required, it was found profitable to arrange for the neutron momentum transfer vector $\mathbf{Q}$ not to be parallel to the phonon wave vector $\mathbf{q}$ but to have a considerable transverse component in such a way that the focusing effect was achieved. Although this sacrifices some over-all integrated intensity by virtue of the $|\mathbf{Q}\cdot\mathbf{e}|^2$ term in the cross section, it produces sharp and well-defined peaks in the scattered-neutron groups.[19] The method cannot be used if there is a transverse phonon branch very close in frequency to the longitudinal branch one is studying. Crystals of zinc set to reflect for the (0002) planes were used for the monochromator and the analyzer. The crystals were treated by quenching them in liquid nitrogen and squeezing them under pressures of up to 3 ton/in.^{2} to increase their mosaic spread. The procedure was optimized by continuing until the integrated elastic peak from a vanadium sample at the sample position reached a maximum. This resulted in crystals of mosaic spreads of up to 0.85° and excellent reflectivities as monochromators.[20] However, it was found that over a period of more than a year the reflectivities of these crystals decreased again somewhat and retreatment was necessary. The collimations used between the source, monochromator, sample, analyzer, and detector were about 40 min arc throughout. The source flux was roughly 3×10^{13} n/cm^2 sec and at 50 meV the flux at the sample position was measured by gold foil activation to be roughly 3.5×10^6 n/cm^2 sec. Although the fast-neutron content in the beam was high, no fast-neutron filters were utilized in the interests of higher thermal fluxes.

The measurements were all carried out in the "constant-Q" mode of operation,[21] and some typical phonon profiles are shown in Fig. 1. The data were analyzed by fitting both the phonon peaks and the background to a series of Gaussians on a uniform background. In this way, part of the contamination of the phonon peaks due to other peaks, such as elastic incoherent peaks, was approximately allowed for. In order to remove possible errors due to asymmetry of the peaks, the centroid of the neutron distribution corresponding to the particular peak in question (i.e., after subtracting off the fitted background) was taken as determining the peak position. In general, these agreed to within 0.02 THz with the position of the fitted Gaussian. The statistical errors in the peak positions were typically 0.02–0.06 THz. All spectrometer angles were set to the nearest 0.01°. No second-order corrections due to finite instrumental resolution were applied to the peak positions. Often, several equivalent measurements of particular phonons were carried out under different conditions, such as in seeking to establish anomalies in a particular branch. In certain cases, there was a systematic deviation in phonon frequencies between different sets of runs, presumably due principally to resolution correction effects. In such cases, the values for the best focused (i.e., narrowest) neutron groups were adopted, so as to minimize such errors. In addition to the purely statistical error in the peak positions, the other main contribution to the errors was due to uncertainty in the exact form of the background to be subtracted from the one-phonon peak, even though these were approximately assumed to be Gaussians. Quite often, spurious peaks due to second order in the analyzer crystal were observed to contaminate the actual phonon peaks.

Table I gives a list of the final set of phonon frequencies determined for the principal symmetry directions of the reciprocal lattice, together with estimated statistical errors. Figure 2 shows a plot of the measured dispersion curves together with fitted force constant model curves to be discussed in Sec. III. It may be seen that the acoustic branches are quite isotropic in the sense that the TA$\parallel$ and TA$\perp$ modes propagating along the $[10\bar{1}0]$ direction are nearly degenerate, as indicated also by the near equality of the elastic constants C_{44} and $\frac{1}{2}(C_{11}-C_{66})$ measured by Smith and Gjevre.[22] It should be noted that, by rotational invariance, the initial slope of the TA$\perp$ mode should be identical also to those of the TA$\perp$ mode along $[11\bar{2}0]$ and the TA modes along [0001]. The longitudinal branch along the $[10\bar{1}0]$ direction also has an initial slope which is only about 2% different from that along the [0001] direction, and, in fact, the two dispersion curves are also almost identical up to the zone boundary along the [0001] direction. The lowest frequency points measured on the acoustic branches are from 3 to 5% different than those predicted from the slopes corresponding to the room-temperature elastic constants, which is not inconsistent with experimental errors and resolution correction effects.[18] It should be noted that the high degree of acoustic isotropy in yttrium is probably fortuitously good at room temperature, since Smith and Gjevre's data show increasing anisotropy of the elastic moduli at lower temperatures. It does, however, reflect the general behavior of most hexagonal metals with a c/a ratio, from ideal hcp ratio,[1–4] and in marked contrast to that of zinc, as noted also by Leake *et al.*[6] for holmium. As in beryllium and magnesium, the LA, LO, TO$\parallel$, and TO$\perp$ modes are almost all degenerate at the symmetry point M. This circumstance makes an uncontaminated determination of these individual modes separately quite

[19] This technique has apparently also been used by the University of Michigan neutron-scattering group [G. Venkataraman (private communication)].

[20] S. W. Peterson, Argonne National Laboratory, Internal Report.

[21] B. N. Brockhouse, in *Inelastic Scattering of Neutrons in Solids and Liquids* (International Atomic Energy Agency, Vienna, 1961), p. 113.

[22] J. F. Smith and J. A. Gjevre, J. Appl. Phys. **31**, 645 (1960).

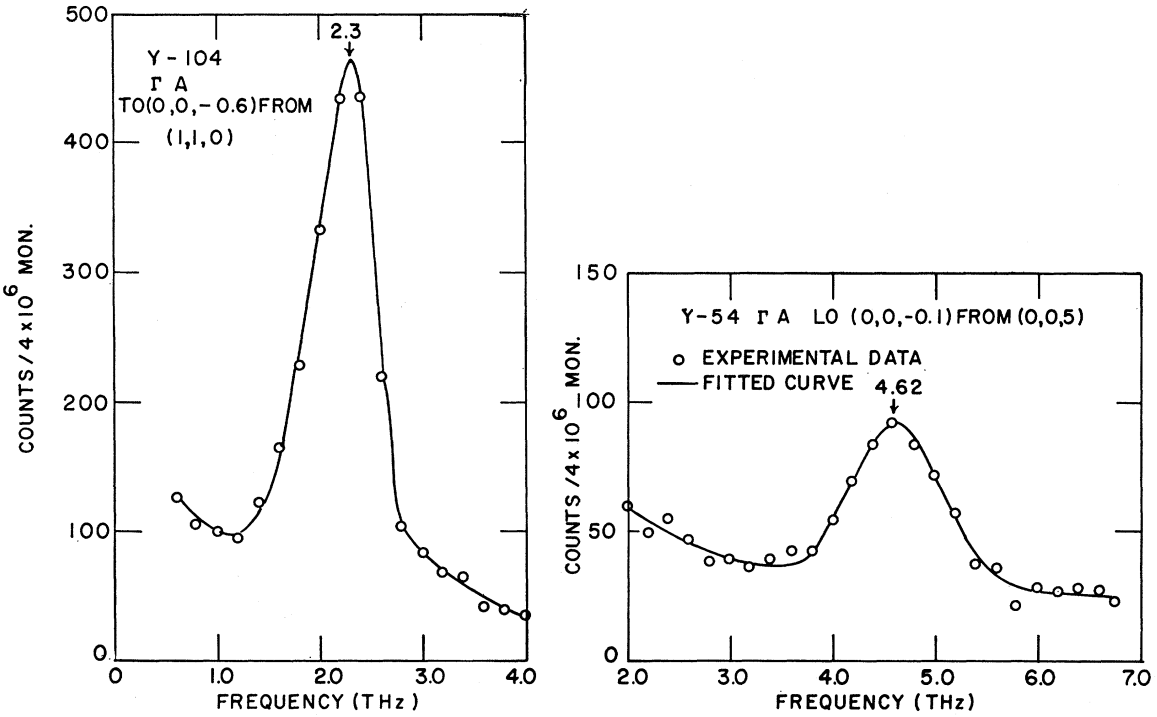

FIG. 1. Representative phonon spectra showing fitted one-phonon peak and background.

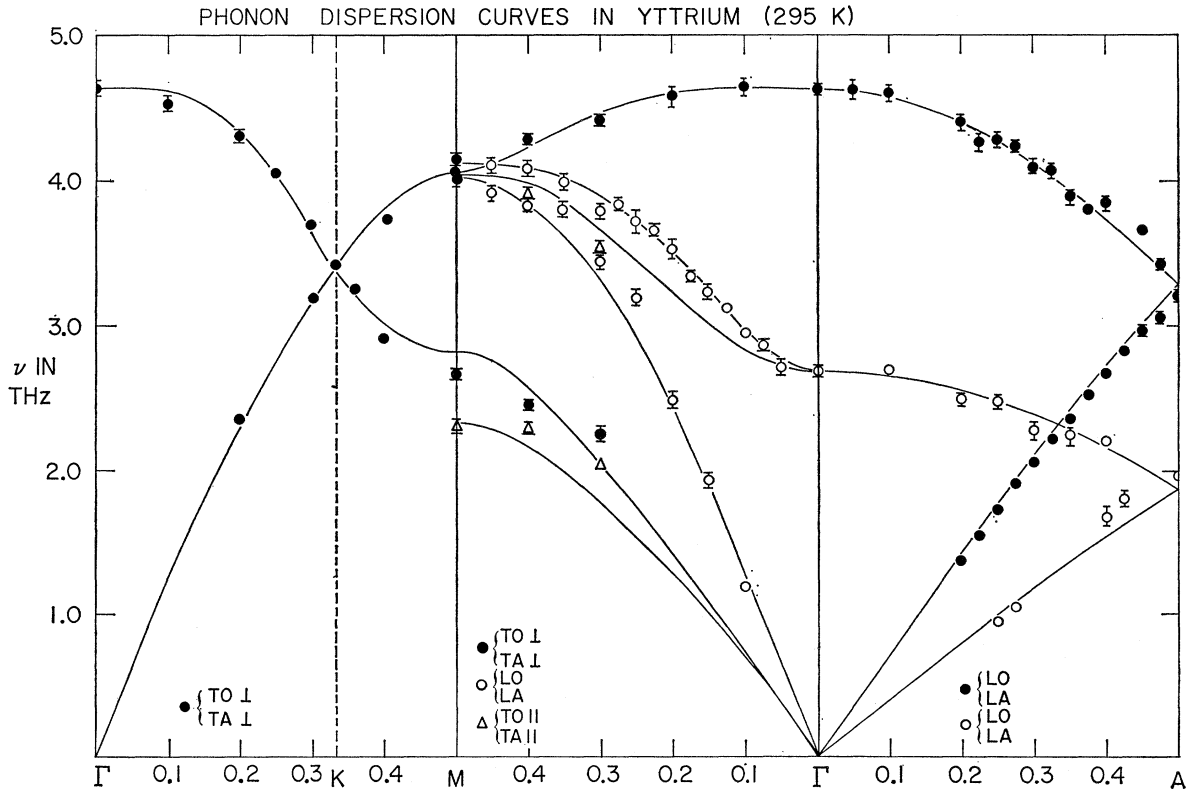

FIG. 2. Phonon-dispersion curves for symmetry directions in yttrium at room temperature. The smooth curves represent the sixth-neighbor MAS model fit. The statistical errors in peak positions are shown as error bars if larger than the size of the points on the figure.

TABLE I. Phonon frequencies in yttrium at 295°K.

$\mathbf{q}=(0,0,\zeta)2\pi/c$

Δ_1(LA)		Δ_2(LO)	
ζ	ν(THz)	ζ	ν(THz)
0.2	1.37±0.02	0.0	4.64±0.05
0.225	1.54±0.02	0.05	4.65±0.06
0.25	1.71±0.02	0.1	4.60±0.05
0.275	1.90±0.02	0.2	4.40±0.05
0.3	2.05±0.02	0.225	4.27±0.05
0.325	2.21±0.02	0.25	4.28±0.05
0.35	2.35±0.02	0.275	4.24±0.04
0.375	2.52±0.02	0.3	4.10±0.05
0.4	2.66±0.02	0.325	4.07±0.05
0.425	2.82±0.03	0.35	3.88±0.04
0.45	2.96±0.03	0.375	3.79±0.03
0.475	3.05±0.03	0.4	3.84±0.04
0.5	3.20±0.04	0.45	3.66±0.02
		0.475	3.42±0.03
Δ_5(TA)		Δ_6(TO)	
ζ	ν(THz)	ζ	ν(THz)
0.25	0.95±0.02	0.0	2.68±0.03
0.275	1.05±0.02	0.1	2.69±0.02
0.4	1.67±0.04	0.2	2.48±0.03
0.425	1.80±0.05	0.25	2.47±0.03
		0.3	2.27±0.05
		0.35	2.23±0.05
		0.4	2.20±0.02
		0.5	1.96±0.02

$\mathbf{q}=(\zeta,0,0)4\pi/\sqrt{3}a$

Σ_1(LA)		Σ_3(TO$\perp$)	
ζ	ν(THz)	ζ	ν(THz)
0.1	1.19±0.02	0.0	4.64±0.05
0.15	1.93±0.05	0.1	4.65±0.06
0.2	2.48±0.06	0.2	4.58±0.06
0.25	3.19±0.06	0.3	4.42±0.04
0.3	3.45±0.06	0.4	4.28±0.04
0.35	3.80±0.05	0.5	4.14±0.04
0.4	3.83±0.04		
0.45	3.91±0.04	Σ_3(TA$\perp$)	
0.5	4.02±0.05	ζ	ν(THz)
		0.3	2.25±0.05
		0.4	2.45±0.03
		0.5	2.67±0.04
Σ_1(LO)		Σ_4(TA$\parallel$)	
ζ	ν(THz)	ζ	ν(THz)
0.0	2.68±0.03	0.3	2.03±0.02
0.05	2.71±0.05	0.4	2.29±0.03
0.075	2.86±0.03	0.5	2.30±0.05
0.1	2.94±0.02		
0.125	3.12±0.03	Σ_4(TO$\parallel$)	
0.15	3.23±0.05	ζ	ν(THz)
0.175	3.33±0.03	0.3	3.53±0.04
0.2	3.53±0.05	0.4	3.90±0.05
0.225	3.66±0.04	0.5	4.04±0.05
0.25	3.72±0.08		
0.275	3.83±0.04		
0.3	3.78±0.05		
0.35	3.99±0.05		
0.4	4.08±0.05		
0.45	4.10±0.05		

$\mathbf{q}=(\zeta,\zeta,0)4\pi/a$

T_3(TA$\perp$)		T_2(TO$\perp$)	
ζ	ν(THz)	ζ	ν(THz)
0.2	2.36±0.02	0.0	4.64±0.05
0.302	3.19±0.02	0.1	4.53±0.05
0.406	3.73±0.03	0.2	4.31±0.03
0.5	4.14±0.04	0.25	4.06±0.02
		0.3	3.69±0.02
		0.333	3.43±0.02
		0.36	3.25±0.02
		0.4	2.91±0.02
		0.5	2.67±0.04

difficult, as may also be seen from inelastic structure factor considerations,[1] and is the reason why relatively few points have been obtained for the TO$\parallel$ branch.

III. FORCE-CONSTANT ANALYSIS

As is well known,[23] the Born–von Kármán theory introduces phenomenological force-constant matrices $\Phi_{\alpha\beta}(\mathbf{l},kk')$ between an atom of basic type k in the origin unit cell and an atom of basis type k' in the unit cell at a lattice vector $\mathbf{l}$ from the origin unit cell. In terms of this completely GTF model, the dynamical matrix whose eigenvalues and eigenvectors are the squares of the phonon frequencies and the phonon polarization vectors, respectively, is given by

$$D_{\alpha\beta}(\mathbf{q},kk')=\sum_{\mathbf{l}} D_{\alpha\beta}(\mathbf{l},kk')e^{-i\mathbf{q}\cdot\mathbf{l}}, \tag{1}$$

where

$$D_{\alpha\beta}(\mathbf{l},kk')=\frac{1}{(m_k m_{k'})^{1/2}}\Phi_{\alpha\beta}(\mathbf{l},kk'), \tag{2}$$

where m_k is the mass of the atom of type k. The most general and complete formulation of the GTF model for hcp crystals has been given by Czachor,[24] and we shall adopt his notation in what follows. In this notation, $k=1$ denotes the sublattice containing the atom situated at the origin of the unit cell and $k=2$ denotes the sublattice containing the atom in the origin unit cell at the position

$$\mathbf{r}=\tfrac{1}{3}\mathbf{a}_1+\tfrac{2}{3}\mathbf{a}_2+\tfrac{1}{2}\mathbf{a}_3,$$

$\mathbf{a}_1$, $\mathbf{a}_2$, and $\mathbf{a}_3$ being the primitive hexagonal-lattice vectors. We have

$$D_{\alpha\beta}(\mathbf{l},11)\equiv-\frac{1}{M}\begin{bmatrix} a & f & e \\ f & b & d \\ e & d & g \end{bmatrix} \tag{3a}$$

and

$$D_{\alpha\beta}(\mathbf{l},12)=D_{\alpha\beta}(\mathbf{l},21)=-\frac{1}{M}\begin{bmatrix} A & F & E \\ F & B & D \\ E & D & G \end{bmatrix}, \tag{3b}$$

where the subscript $\mathbf{l}$ is understood for the force constants and M is the mass of an atom of the lattice.

Strictly speaking, the lack of inversion symmetry without a nonprimitive translation complicates the analysis considerably since $D_{\alpha\beta}(\mathbf{l},22)$ is not equal to $D_{\alpha\beta}(\mathbf{l},11)$. Hence, Czachor splits the force constants between like atoms (denoted by the lower-case letters a, b, etc.) into "symmetric" and "antisymmetric" independent force constants, i.e.,

$$D_{\alpha\beta}(\mathbf{l},11)=D_{\alpha\beta}{}^{s}(\mathbf{l},11)+D_{\alpha\beta}{}^{a}(\mathbf{l},11), \tag{4}$$

such that

$$D_{\alpha\beta}{}^{s}(\mathbf{l},11)+D_{\alpha\beta}{}^{a}(\mathbf{l},22)=D_{\alpha\beta}{}^{s}(\mathbf{l},22)-D_{\alpha}{}^{a}(\mathbf{l},22). \tag{5}$$

[23] M. Born and K. Huang, *Dynamical Theory of Cryatal Lattices* (Oxford University Press, Fair Lawn, N. J., 1954).

[24] A. Czachor, in *Inelastic Scattering of Neutrons in Solids and Liquids* (International Atomic Energy Agency, Vienna, 1965), Vol. I, p. 181.

The antisymmetric force constants do not appear in the dynamical matrix for the special modes along the symmetry directions which we have measured, and, hence, are not directly determinable. Fortunately, the MAS model of DeWames *et al.* simplifies the analysis by putting all of these equal to zero, so that $D_{\alpha\beta}(\mathbf{1},11) = D_{\alpha\beta}(\mathbf{1},22)$, which is physically reasonable in the case that the force constant between atoms is a function only of their distance apart. Certain of the off-diagonal elements of the $D_{\alpha\beta}(\mathbf{1},kk')$ also do not appear in the expressions for the special modes measured. However, the MAS model enables one to express them in terms of the diagonal elements alone, leaving, in general, only three independent force constants per neighbor atom. In the Appendix, we list the coordinates of the typical atoms in each successive ring of neighbors to which our force constants refer, together with the restrictions imposed by crystalline symmetry and the additional restrictions imposed by the MAS model, and finally the independent force constant parameters for each atom. For detailed discussions and other applications of the MAS model, the reader is referred to the papers of DeWames *et al.*[15] and Raubenheimer and Gilat.[17] It may be seen that a fourth-neighbor model involves 11 independent parameters. It was found that solving for these parameters in terms of suitably chosen frequencies at symmetry points and the elastic constants was not satisfactory in the sense that it was not possible to get a good fit to the dispersion curves and simultaneously describe correctly the behavior in the elastic limit, i.e., either satisfy the rotational invariance condition (discussed below) or fit the elastic constant C_{13}, describing the elastic behavior in off-symmetry directions. A sixth-neighbor model involves 17 independent parameters, but a least-squares fitting procedure proved to be unsatisfactory because of convergence difficulties and problems in ensuring that the parameters were unique.

In order to avoid these difficulties, the following procedure was adopted. It is well known for monatomic crystals, e.g., cubic crystals, that a Fourier analysis of $\omega_j^2(\mathbf{q})$ for symmetry direction modes yields information both about the range of the forces as well as a number of linear relations among the interatomic force constants.[25] For the hcp lattice, the situation is more complex, but the Fourier analysis of ω^2(LA,LO) and ω^2(TA,TO) along the ΓA direction (with the double-zone scheme convention adopted so that the (LA,LO) branches are regarded as one "acoustic" branch and so on), of $\omega^2(\mathrm{TA}\perp)$ and $\omega^2(\mathrm{TO}\perp)$ along the ΓKM direction, and of the *sums* of ω^2 for branches of like symmetry along the ΓM direction still yield coefficients which are *linear* combinations of the interatomic force constants. The results of such an analysis are shown in Table II, where we show the Fourier coefficients fitted consistent with an interaction up to sixth neighbors, together with the minimum number of coefficients needed to obtain a good fit for each branch. In the Appendix, we list these coefficients as linear combinations of interatomic force constants out to sixth neighbors. An inspection of this list and Table II shows that, as far as coefficients involving the zz-component force constants (i.e., the g's and G's), a third-neighbor model would represent these coefficients reasonably well, but that the basal plane interactions (i.e., the a's, b's, A's, and B's) must be included up to at least sixth neighbors. (In fact, the analysis of the longitudinal ΓM branches shows that, strictly speaking, Fourier coefficients involving even longer-range interactions are present.) Using the Fourier coefficients listed in Table II, the measured elastic moduli, $(C_{11}-C_{66})$, C_{33}, C_{44}, $(C_{13}+C_{44})$, and the expressions for the frequencies of the LA, LO, TA||, and TO|| modes at M, we have 28 linear relations between the 17 force-constant parameters (as listed in the Appendix) and have determined the latter by a linear least-squares fitting procedure. However, although a good fit was obtained, such a fit did not give a good representation of the elastic constant C_{11}, which is not a linear combination of force constants. This was traced to the behavior of the force constants A_1, B_1, A_2, B_2, A_3, B_3. In order to get a final model, therefore, we chose the remaining force constants as determined from the linear least-squares fit, and solved for A_1, B_1, A_2, B_2, A_3, B_3 in terms of $(A_1+B_1+A_2+B_2+2A_3+2B_3)$ as determined from the same fit, $(C_{11}-C_{66})$, $(C_{13}+C_{44})$, the frequencies of the LA and TO|| modes at M, and C_{11}. As may be seen from the table of linear relations in the appendix, such

TABLE II. The notation for the Fourier coefficients is explained in the Appendix. Units are in 10^4 dyn/cm.

Function	Fourier coefficient	Value	Minimum number needed for fit
ΓA direction:			
$m\omega_{(\mathrm{LA})}^2$	P_1	6.2984	1
	P_2	−0.0078	1
$m\omega_{(\mathrm{TA})}^2$	P_1	2.1462	1
	P_2	−0.0357	1
ΓKM direction:			
$m\omega^2(\mathrm{TA}\perp)$	P_1	4.6042	3
	P_2	−0.04689	3
	P_3	0.06244	3
$m\omega^2(\mathrm{TO}\perp)$	P_0	8.8534	4
	P_1	4.3509	4
	P_2	−0.7022	4
	P_3	−0.1748	4
ΓM direction:			
$m\omega^2(\mathrm{LA})+m\omega^2(\mathrm{LO})$	P_0	12.412	>3
	P_1	−7.6148	>3
	P_2	−0.7800	>3
$m\omega^2(\mathrm{TA}\perp)+m\omega^2(\mathrm{TO}\perp)$	P_0	13.7332	3
	P_1	−0.7740	3
	P_2	−0.4104	3
$m\omega^2(\mathrm{TA}\parallel)+m\omega^2(\mathrm{TO}\parallel)$	P_0	8.3936	2
	P_1	−4.2396	2
	P_2	0.03088	2

[25] A. J. E. Foreman and W. M. Lomer, Proc. Phys. Soc. (London) **70**, 1143 (1957).

TABLE III. Force constants for the sixth-neighbor MAS model. Units are in dyn/cm.

Neighbor	GTF notation	MAS notation
1	$A_1 = 4513.1$	$\delta_1 = 2047.2$
	$B_1 = 418.8$	$\epsilon_{1x} = -1628.4$
	$G_1 = 11518.7$	$\epsilon_{1z} = -3640.7$
2	$a_1 = 3986.7$	$\alpha_2 = 10124.0$
	$b_1 = 9048.7$	$\beta_{2x} = 1455.7$
	$g_1 = 510.36$	$\beta_{2z} = 510.36$
3	$A_2 = 1211.5$	$\delta_3 = -273.15$
	$B_2 = -3159.0$	$\epsilon_{3x} = 1211.5$
	$G_2 = -512.16$	$\epsilon_{3z} = 1510.6$
4	$a_2 = -178.3$	$\beta_{4x} = -178.3$
	$g_2 = -83.0$	$\alpha_4 + \beta_{4z} = -83.0$
5	$A_3 = 928.0$	$\delta_5 = 39.31$
	$B_3 = 1085.2$	$\epsilon_{5x} = 456.3$
	$G_3 = -290.9_5$	$\epsilon_{5z} = -582.0$
6	$a_3 = -93.00$	$\alpha_6 = 1855.9$
	$b_3 = 1762.9$	$\beta_{6x} = -93.00$
	$g_3 = 592.7$	$\beta_{6z} = 592.7$

a procedure cannot destroy the goodness of fit for any of the coefficients listed there except for possibly the frequencies of the LO and TA$\|$ modes at M. The force constants so obtained are listed in Table III together with the equivalent force constants in the MAS notation.[15] Figure 2 shows the fit obtained to the dispersion curves with such a model, and it may be seen that by and large the agreement is fairly good, except for the TA branches along ΓM where the maximum discrepancy is 15%. The fit to all the elastic constants ensures that the model has the right behavior at small wave vector for all directions including off-symmetry directions. Another test of the model is to see whether it satisfies the condition of rotational invariance,[24] which ensures that the initial slope of the TA$\perp$ mode along ΓM is equal to that of the TA mode along ΓA. This is expressed as a relation between the force constants in the Appendix. The model obtained by us satisfies this condition to within 2%.

Using this sixth-neighbor MAS model and the HCPGNU program developed by Raubenheimer and Gilat,[17] we have calculated the frequency spectrum of the yttrium lattice as is shown in Fig. 3. Some of the critical points corresponding to symmetry direction measurements are also indicated on this figure. The spectrum resembles qualitatively that of magnesium as calculated by Gilat and Raubenheimer using the fourth-neighbor model of Iyengar *et al.*[1] but there are significant differences, showing that our sixth-neighbor model predicts rather different behavior in the off-symmetry directions even though the symmetry direction dispersion curves in the two metals are rather similar. From our frequency spectrum, we have calculated a lattice specific

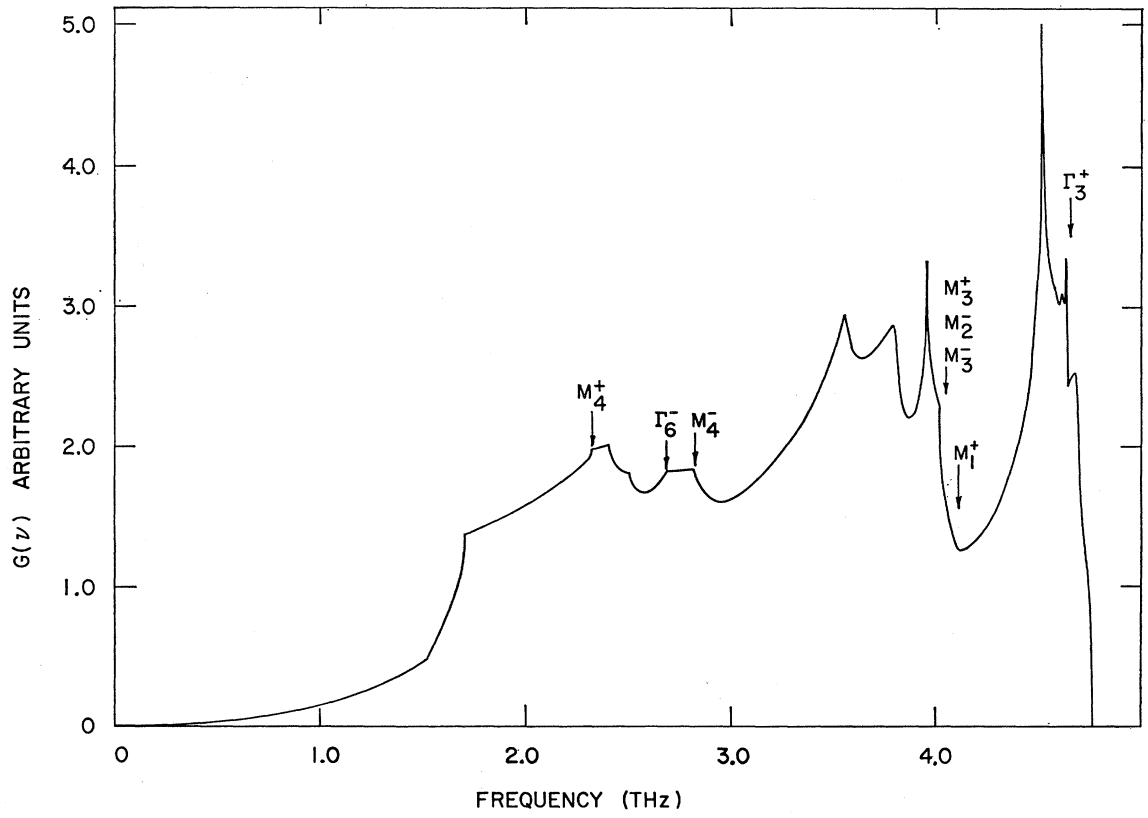

FIG. 3. Frequency spectrum $g(\nu)$ for yttrium showing critical points arising from symmetry directions only.

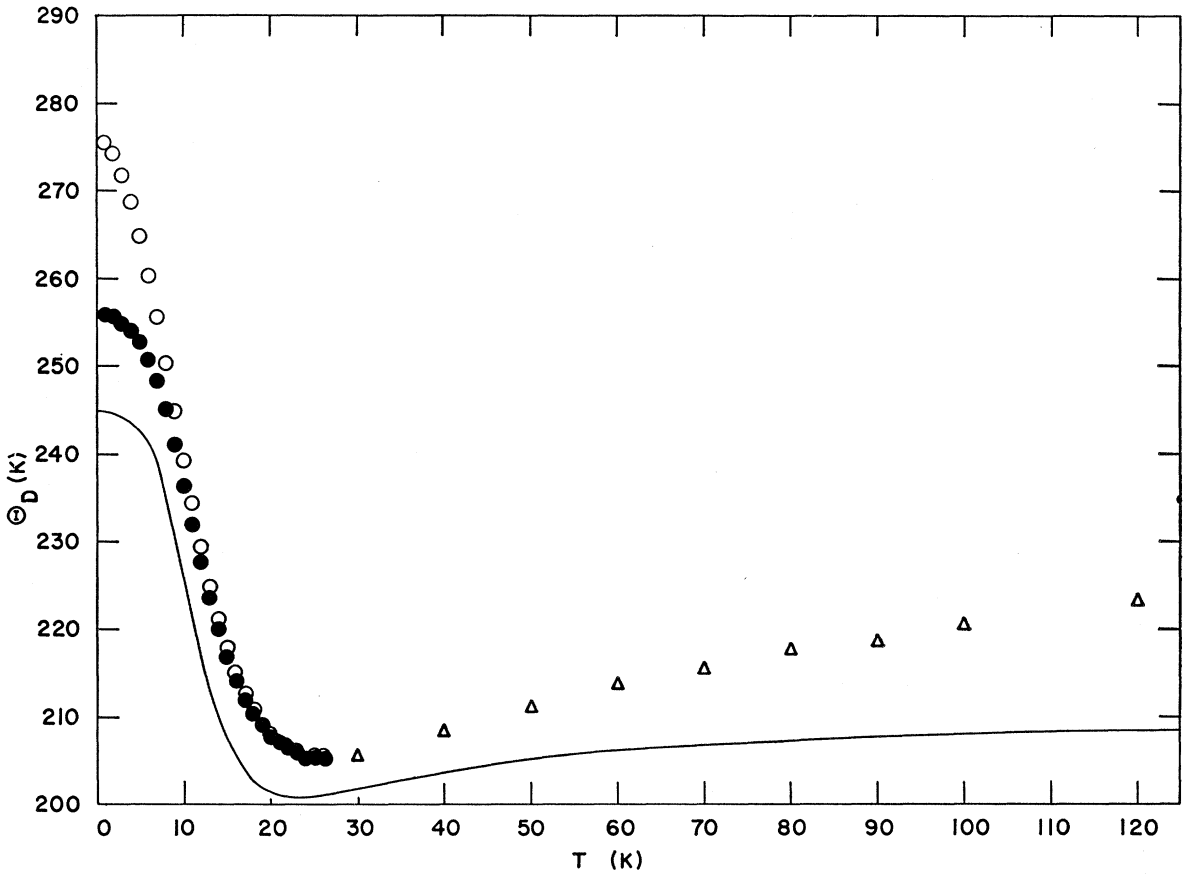

FIG. 4. Plot of Debye temperature versus T for yttrium calculated from $g(\nu)$ shown in Fig. 3, together with experimental data of Cetas, Holste, and Swenson and of Jennings, Miller, and Spedding. The full circles represent data of Cetas *et al.* fitted by forcing $\theta(0)$ to be consistent with the low-temperature elastic constants. The open circles represent their data fitted with no such restriction, and the triangles represent the data of Jennings *et al.*

heat and used it to obtain a Debye Θ as a function of temperature for yttrium. This is shown in Fig. 4 together with the experimental data of Cetas *et al.*[26] for low temperatures and of Jennings *et al.*[27] for higher temperatures. It may be seen that, in general, our calculations are in good agreement with these data and reproduce the dip in the Θ-T curve very well, considering the fact that our calculations are based on a room-temperature spectrum that will change slightly at lower temperatures and that there are difficulties in estimating the appropriate parameters to convert the experimentally measured Cp to a lattice Debye Θ. The low temperature data of Cetas *et al.* is slightly ambiguous, owing to the fact that they have eliminated other specific heat contributions in two different ways resulting in two different sets of Θ's at very low temperatures. Their lower curve is in agreement with the Θ calculated from the low-temperature elastic constants of Smith and Gjevre.[22] We have found that any force model which does not reproduce the elastic constant C_{13} gives a Θ-T curve with a completely wrong behavior at very low temperatures.

We have also used our model to calculate the Debye-Waller factor for yttrium. For an hcp crystal, this may be written as

$$\exp(-2W)=\exp\{-(\hbar^2/2M)[(K_{\parallel}^2/k_B\Theta_0)G_{\parallel}(T/\Theta_0)+(K_{\perp}^2/k_B\Theta_0)G_{\perp}(T/\Theta_0)]\}, \quad (6)$$

where M is the atomic mass, $(\hbar K_{\parallel})$ and $(\hbar K_{\perp})$ are the components of momentum transfer parallel and perpendicular to the basal plane, respectively, and Θ_0 is some reference Debye temperature which we shall take to be the Θ at 0°K. The point of writing e^{-2W} in the form (6) is that since the frequencies of the rare-earth metals including yttrium approximately scale in the ratio of their Θ_0's, $G_{\parallel}(T/\Theta_0)$ and $G_{\perp}(T/\Theta_0)$ may be taken to be universal dimensionless functions from which one may calculate e^{-2W} for any of the metals in this series. This may be found to be useful in certain neutron-diffraction experiments where occasionally accurate anisotropic

[26] T. C. Cetas, J. C. Holste, and C. A. Swenson, Phys. Rev. **182**, 679 (1969).
[27] L. D. Jennings, R. E. Miller, and F. H. Spedding, J. Chem. Phys. **33**, 1849 (1960).

TABLE IV. The dimensionless functions $G_{\parallel}(T/\Theta_0)$ and $G_{\perp}(T/\Theta_0)$ appearing in Eq. (6) for the Debye-Waller factor.

T/Θ_0	$G_{\parallel}(T/\Theta_0)$	$G_{\perp}(T/\Theta_0)$
0.05	1.883_5	1.920
0.10	3.873	3.956
0.15	6.056	6.209
0.20	8.504	8.752
0.25	11.263	11.633
0.3	14.364	14.881
0.35	17.821	18.507
0.4	21.647	22.531
0.45	25.862	26.969
0.5	30.474	31.828
0.6	40.908	42.832
0.7	52.982	55.575
0.8	66.717	70.077
0.9	82.126	86.353
1.0	99.218	104.41
1.2	138.48	145.90
1.4	184.54	194.59
1.6	237.42	250.50
1.8	296.43	312.66
2.0	361.88	381.97

Debye-Waller factors are needed. Table IV gives a tabulation of the functions $G_{\parallel}$ and $G_{\perp}$ for certain values of (T/Θ_0).

IV. ELECTRON-PHONON INTERACTION IN YTTRIUM

The conduction-electron band structure of yttrium is known to be transition-metal-like, in the sense that it consists of overlapping s-like and d-like bands.[7] Hence, a simple pseudopotential approach to the electron-phonon interaction as is used in the free-electronlike metals is inapplicable. The formulation of the electron-phonon interaction and the electronic contribution to the dynamical matrix for transitionlike metals has been given by Sinha.[11] A detailed calculation for yttrium however would require a knowledge of the wave functions and energy levels for a large number of bands which are not yet available. However, the formulation does show that the electronic contribution to the dynamical matrix is governed by terms having the usual second-order perturbation form

$$\sum_{k,k'}{}' \frac{n(k)-n(k')}{E_k-E_{k'}} |V_{kk'}|^2, \tag{7}$$

where $V_{kk'}$ is the electron-phonon matrix element between states k and k' with occupation numbers $n(k)$, $n(k')$ and energies E_k, $E_{k'}$. For phonon wave vector $\mathbf{q}$, the Bloch wave vectors of the two states are related by

$$\mathbf{k}'=\mathbf{k}+\mathbf{q}. \tag{8}$$

For more than one atom per unit cell, $V_{k'k}$ includes a structure factor which, in the case of the hcp lattice, imposes the extra selection rule that Eq. (8) is to be assumed only for wave vectors in the double-zone scheme (i.e., with the Brillouin zone considered to be twice as large along the c axis as the normal Brillouin zone). In this scheme, phonon wave vectors for the acoustic branches along ΓA have $\mathbf{q}$'s between Γ and A and those for optic branches have $\mathbf{q}$'s between A and Γ in the second zone.

For a transition across the Fermi surface, the expression (7) becomes infinite, but this infinity is in general cancelled by neighboring contributions so that a principal-value-type sum remains. An exception is where $\mathbf{q}$ spans an extremal dimension of the Fermi surface, in which case one gets *singularities* in the $\mathbf{q}$ dependence of Eq. (7) for that $\mathbf{q}$ resulting in the well-known Kohn-type anomalies in the dispersion curves.[10,28] The nature of these singularities depends on the geometry of the Fermi surface in this region and can range from an actual infinity in (7) to an infinity in its derivative with respect to $\mathbf{q}$. If, on the other hand, one does not have an actual extremum but rather a region of Fermi surface consisting of two pieces of relatively large area separated by approximately the same $\mathbf{q}$, i.e., the so-called "nested" Fermi surfaces,[29] then it is possible for the expression (7) to build up into a large peak without an actual singularity. Figure 5 illustrates a plot of the function $\chi(\mathbf{q})$ defined as

$$\chi(\mathbf{q})=\sum_{k} \frac{n(\mathbf{k})-n(\mathbf{k}+\mathbf{q})}{E_{\mathbf{k}}-E_{\mathbf{k}+\mathbf{q}}} \tag{9}$$

for yttrium where only the third and fourth bands which contribute to the Fermi surface were taken into account in the sum. This curve is from the work of Gupta *et al.*[30] It shows three broad peaks (two of which are not resolved) at $\mathbf{q}=(0,0,\zeta)2\pi/c$ ($\zeta=0.375$, 0.583, and 0.75 approximately). These peaks may be correlated with various nested portions of the Fermi surface of yttrium along the c axis, as calculated by Loucks.[7] One may expect that the peaks in $\chi(\mathbf{q})$ might correspond to dips in the dispersion curves particularly for the longitudinal branches along the ΓA direction, even though the matrix elements have been omitted in Eq. (9) and not all bands summed over. Yttrium is not a superconductor so that the electron-phonon interaction is probably not very large, and, hence, the magnitude of the effect is expected to be small. Accordingly, a very careful search was made for such effects along the LA and LO branches of the dispersion curve along ΓA including measurements for a large number of closely spaced $\mathbf{q}$ values and repeated sets of runs for the same $\mathbf{q}$ from different reciprocal lattice points, using high resolution and focusing where possible. The results indicate that the Δ(LA) branch is quite smooth all the way to the zone boundary but that the Δ(LO) branch does seem to have two sharp dips at the positions $(0,0,0.625)2\pi/c$ and $(0,0,0.775)2\pi/c$ in the double-zone

[28] L. M. Roth, H. J. Zeiger, and T. A. Kaplan, Phys. Rev. **149**, 519 (1966).
[29] T. L. Loucks, Int. J. Quantum Chem. **11S**, 285 (1968).
[30] R. P. Gupta, S. H. Liu, and S. K. Sinha (unpublished).

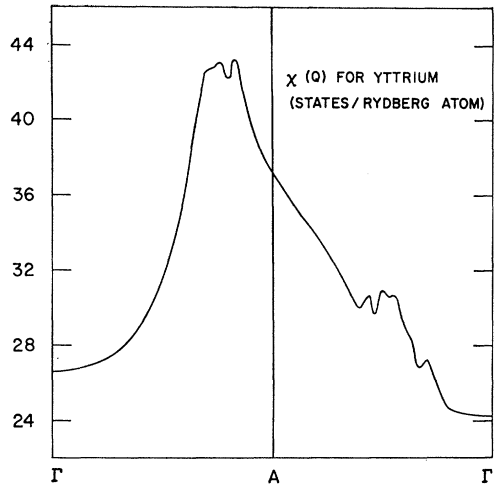

FIG. 5. The function $\chi(Q)$ for yttrium calculated using Eq. (9) and the approximations mentioned in the text, in the double-zone representation.

representation. Even though the magnitude of these dips is comparable with the over-all experimental error, the evidence for them is obtained from the fact that the dispersion curve for this branch as measured from each independent set of runs showed these same two dips even though the curves obtained from each set were shifted up or down relative to each other because of systematic error. We feel that these two points, then, are likely candidates for the points corresponding to the second and third peaks in Fig. 5. The small discrepancies in positions may be due to the effects of the matrix elements or to errors in the Fermi surface dimensions. There appear to be a couple of other anomalies in the dispersion curves such as along the TA and TO branches along ΓA and the LO branch along ΓM. However, it is difficult to exclude the possibility of contamination of these branches by peaks resulting from neighboring branches of the dispersion curve and we have not attempted to establish any of these in the same way as for the Δ(LO) and Δ(LA) branches.

The lack of an anomaly due to the biggest peak in $\chi(\mathbf{q})$ at $(0,0,0.375)2\pi/c$ is disturbing in view of the fact that the existence of this peak can be correlated with the magnetic ordering in dilute rare-earth alloys with yttrium.[31,32] The neutron-diffraction results of Koehler *et al.*[33] indicate a $\mathbf{q}$ value for the magnetic ordering wave vector in these alloys in the extremely dilute rare-earth limit of $(0,0,0.283)2\pi/c$, which is close to the $\mathbf{q}$ value of the first peak in $\chi(\mathbf{q})$. The argument is qualitative since again the $\chi(\mathbf{q})$ which determines the magnetic ordering should have the appropriate *s-f* exchange matrix elements in the expression in Eq. (9).[32] The complete absence of a corresponding anomaly in the phonon spectrum may be ascribed either to cancellation of this effect by other terms in the total electronic contribution to the dynamical matrix or to the fact that the appropriate nesting feature in the Fermi surface yttrium is not quite as pronounced as the calculations indicate. It should be noted that a similar dip has been seen in the magnon spectrum of an $Ho_{0.1}Tb_{0.9}$ alloy by Møller *et al.*[34] corresponding to the *optical* branch along ΓA, but not at the $\mathbf{q}$ corresponding to the magnetic ordering wave vector, even though Møller *et al.* have shown that the results are consistent with having a peak in $\chi(\mathbf{Q})$ between Γ and A.

V. SUMMARY AND DISCUSSION

We have presented measurements of the phonon dispersion relations in yttrium at 295 K utilizing the technique of coherent inelastic scattering of thermal neutrons. The measurements are restricted to the principal symmetry modes, but even these have necessitated a complicated force-constant model in order to obtain a good fit. We have developed a technique of obtaining the parameters of a sixth-neighbor MAS model linearly from a Fourier analysis of the dispersion curves together with the values of the measured elastic constants. The force constants so obtained are unique, and we believe the model represents the dispersion curves over the whole Brillouin zone reasonably well, as the frequency spectrum calculated from it yields a Θ-T curve in reasonably good agreement with the experiment. We believe this represents one of the most detailed force-constant analyses reported on an hcp metal and in particular on a rare-earth–type metal. Sundström[35] has reported a detailed application of a third-neighbor axially symmetric model to the heavy rare-earth metals by fitting the measured elastic constants. As she had no access to phonon dispersion curve measurements, the agreement of her model with the details of the phonon spectra is uncertain. Her calculated frequency spectrum does not look very similar to the one calculated by us for yttrium. Very recently, Lahteenkorva[36] has reported similar model calculations for yttrium. We have also presented a calculation of the Debye-Waller factor which may be used to obtain realistic Debye-Waller factors for the rare-earth metals with the use of appropriate scaling factors.

We have searched quite hard for evidence of Fermi-surface effects manifested through the electron-phonon interaction. Such effects have proved to be rather disappointingly small indicating that the electron-phonon interaction is not particularly strong in this metal. A large anomaly in the Δ(LA) branch predicted

[31] S. C. Keeton and T. L. Loucks, Phys. Rev. **168**, 672 (1968).
[32] W. E. Evenson and S. H. Liu, Phys. Rev. **178**, 783 (1969).
[33] W. C. Koehler, H. R. Child, E. O. Wollan, and J. W. Cable, J. Appl. Phys. **34**, 1335 (1963).
[34] H. Bjerrum Møller, J. C. G. Houmann, and A. R. Mackintosh, Phys. Rev. Letters **19**, 312 (1967).
[35] Lorna Sundström, Ann. Acad. Sci. Fennicae **A VI**, 280 (1968).
[36] E. E. Lahteenkorva (private communication).

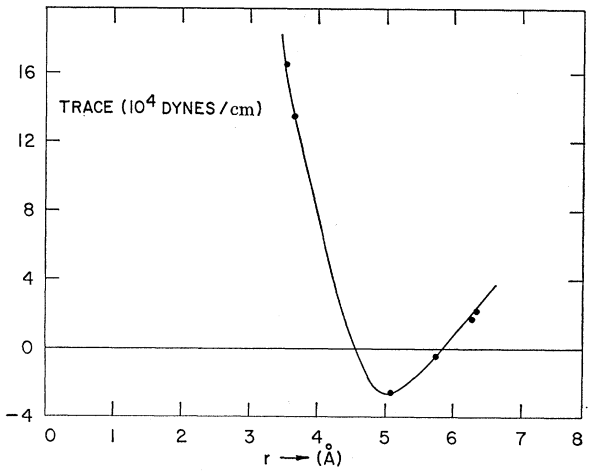

FIG. 6. Plot of the quantity

$$\sum_{\alpha} \phi_{\alpha\alpha}\binom{l}{kk'}$$

as a function of neighbor distance.

by theoretical calculations of the generalized susceptibility function has not been observed indicating that the magnitude of the peak in $\chi(\mathbf{q})$ may not be as large as the calculations suggest. It is interesting to observe the behavior of the *traces* of our fitted force constant matrices [i.e., the quantities $(a+b+g)$ or $(A+B+G)$] as a function of neighbor distance. It is well known[25,37] that the trace of a force constant matrix reflects only the non-Coulombic contributions to the interactions associated with that particular neighbor, i.e., forces due to the ion-electron-ion interaction only. The traces of the force-constant matrices in real space may be viewed accordingly as a Fourier representation of the sum rule for $\sum_j \omega_j^2(\mathbf{q})$ proposed by Rosenstock.[37] Figure 6 shows the trace as a function of neighbor distance. It may be seen that the points seem to lie on a smooth curve exhibiting oscillatory behavior. This is probably a reflection of the Friedel-type oscillations such as are also seen in the simple metals.[38] It may also be noticed that there is almost no interaction between the origin atom and its fourth neighbors at positions $(0, 0, \pm c)$. This may be interpreted either as indicating directional bonding between atoms preferentially off the c axis, i.e., lack of electron orbitals directed along the c axis if one crudely thinks of the d electrons in terms of the linear-combination-of-atomic-orbitals wave functions, or simply as due to the fact that the ion-electron-ion interaction is near zero for that particular distance.

It is obvious that a calculation taking the conduction electrons into account properly is required for this type of metal. Models taking the electron gas into account phenomenologically[39] or by making approximations appropriate to free electrons and using pseudopotential theory are not expected to work in this case, and are not even altogether satisfactory for the simple hcp metals.[40,41] Gupta's[42] calculations for yttrium yield a disagreement of 15–20% with experiment. Phenomenological models including angular forces[43,44] may give better agreement with fewer parameters.

ACKNOWLEDGMENTS

It is a pleasure to thank Dr. R. W. Williams for providing us with the single-crystal sample used in the experiment, and the Oak Ridge inelastic scattering group for supplying the HCPGNU program used in the frequency spectra calculation. We wish to acknowledge stimulating discussions with Dr. T. L. Loucks, Dr. J. L. Stanford, and Dr. S. H. Liu on the Fermi-surface effects and are grateful to Dr. R. P. Gupta for the $\chi(\mathbf{q})$ calculations for yttrium. It is also a pleasure to acknowledge Dr. A. R. Mackintosh for his initial help and encouragement in setting up the triple-axis spectrometer and in the early phase of this work. We have also benefited from helpful discussions with Dr. N. Wakabayashi and Dr. F. H. Spedding.

APPENDIX

We list below the coordinates of the typical atoms in each neighbor ring to which the force-constant matrices, as defined generally in Eqs. (3), are assumed to refer to. The atom at the origin is assumed to belong to sublattice $k=1$. A Cartesian coordinate system is chosen with the x axis along the a axis of the crystal and the z axis along the c axis.

Neighbors on Sublattice $k=1$

Neighbor	Coordinates	Restrictions imposed by crystal symmetry	Further MAS restrictions	Independent parameters
2nd	$(\frac{1}{2}a,\frac{1}{2}\sqrt{3}a,0)$	$d_1=e_1=0$; $f_1=-\frac{1}{2}\sqrt{3}(a_1-b_1)$	All antisymmetric force constants vanish	a_1, b_1, g_1
4th	$(0,0,c)$	$d_2=e_2=f_2=0$; $b_2=a_2$		a_2, g_2
6th	$(0,\sqrt{3}a,0)$	$d_3=e_3=f_3=0$		a_3, b_3, g_3

[37] H. B. Rosenstock, Phys. Rev. **129**, 1959 (1963).
[38] S. H. Koenig, Phys. Rev. **135**, A1693 (1964).
[39] R. P. Gupta and B. Dayal, Phys. Status Solidi **8**, 115 (1965).
[40] V. C. Sahni and G. Venkataraman, Phys. Rev. **185**, 1002 (1969).
[41] A. Czachor, Phys. Status Solidi **29**, 423 (1968).
[42] R. P. Gupta, Phys. Status Solidi **20**, 291 (1967); and (private communication).
[43] Y. P. Varshni and P. S. Yuen, Phys. Rev. **174**, 766 (1968).
[44] E. A. Metzbower, Phys. Rev. **177**, 1139 (1969).

Neighbors on Sublattice $k=2$

Neighbor	Coordinates	Restrictions imposed by crystal symmetry	MAS restrictions	Independent parameters
1st	$(\frac{1}{2}a,a/2\sqrt{3},\frac{1}{2}c)$	$E_1=\sqrt{3}D_1$; $F_1=\frac{1}{2}\sqrt{3}(A_1-B_1)$	$D_1=\frac{1}{2}\sqrt{3}\gamma(A_1-B_1)$	A_1, B_1, G_1
3rd	$(0,2a/\sqrt{3},\frac{1}{2}c)$	$E_2=F_2=0$	$D_2=\frac{1}{4}\sqrt{3}\gamma(B_2-A_2)$	A_2, B_2, G_2
5th	$(a,(2/\sqrt{3})a,\frac{1}{2}c)$	None	$F_3=2\sqrt{3}(B_3-A_3)$; $E_3=\frac{3}{2}\gamma(B_3-A_3)$; $D_3=\frac{1}{2}\gamma F_3$	A_3, B_3, G_3

where $\gamma=c/a$. In terms of the above parameters, we write down below the relations between the Fourier coefficients and the elastic constants on one side and the force constants up to sixth neighbors on the other. The notation $P_1(\mathrm{LA})$ will indicate the first Fourier coefficient of $M\omega^2$ for an LA branch, for instance, whereas $P_0(\mathrm{LA+LO})$ will indicate the zeroth Fourier coefficient of $M\omega_{\mathrm{LA}}{}^2+M\omega_{\mathrm{LO}}{}^2$, i.e., the constant term. Along the ΓA direction, the double-zone representation is assumed so that the (LA,LO) branches unfolded are assumed to form one LA branch, and similarly for the (TA,TO) branches.

ΓA direction:

$$P_1(\mathrm{LA})=6G_1+6G_2+12G_3,$$
$$P_2(\mathrm{LA})=2g_2,$$
$$P_1(\mathrm{TA})=3A_1+3B_1+3A_2+3B_2+6A_3+6B_3,$$
$$P_2(\mathrm{TA})=2a_2.$$

ΓKM direction:

$$P_1(\mathrm{TA}\perp)=4g_1+4G_1+4G_3,$$
$$P_2(\mathrm{TA}\perp)=2g_1+4G_2+4G_3,$$
$$P_3(\mathrm{TA}\perp)=4g_3+4G_3,$$
$$P_0(\mathrm{TO}\perp)=6g_1+4g_3+8G_1+8G_2+12G_3,$$
$$P_1(\mathrm{TO}\perp)=-4g_1+4G_1+4G_3,$$
$$P_2(\mathrm{TO}\perp)=-2g_1+4G_2+4G_3,$$
$$P_3(\mathrm{TO}\perp)=-4g_3+4G_3.$$

ΓM direction:

$$P_0(\mathrm{TA}\perp+\mathrm{TO}\perp)=8g_1+12g_3+12G_1+12G_2+24G_3,$$
$$P_1(\mathrm{TA}\perp+\mathrm{TO}\perp)=-8g_1-8g_3,$$
$$P_2(\mathrm{TA}\perp+\mathrm{TO}\perp)=-4g_3,$$
$$P_0(\mathrm{TA}\parallel+\mathrm{TO}\parallel)=8a_1+6a_3+6b_3+6A_1+6B_1+6A_2+6B_2+12A_3+12B_3,$$
$$P_1(\mathrm{TA}\parallel+\mathrm{TO}\parallel)=-8a_1-2a_3-6b_3,$$
$$P_2(\mathrm{TA}\parallel+\mathrm{TO}\parallel)=-4a_3,$$
$$P_0(\mathrm{LA+LO})=8b_1+6a_3+6b_3+6A_1+6B_1+6A_2+6B_2+12A_3+12B_3,$$
$$P_1(\mathrm{LA+LO})=-8b_1-6a_3-2b_3,$$
$$P_2(\mathrm{LA+LO})=-4b_3.$$

Elastic constants:

$$2\sqrt{3}c(C_{11}-C_{66})=-12a_1+12b_1-18a_3+18b_3+4A_1-4B_1-8A_2+8B_2-196A_3+196B_3,$$
$$a(C_{13}+C_{44})/(\sqrt{3}\gamma)=2A_1-2B_1-A_2+B_2-14A_3+14B_3,$$
$$\sqrt{3}a^2C_{33}/c=4g_2+3G_1+3G_2+6G_3,$$
$$c\sqrt{3}C_{44}/2=3g_1+9g_3+G_1+4G_2+14G_3.$$

Frequencies at M:

$$m\omega_{\mathrm{LA(LO)}}{}^2=8b_1+6a_3+2b_3+8B_1+12A_3+4B_3,$$
$$m\omega_{\mathrm{LO(LA)}}{}^2=8b_1+6a_3+2b_3+6A_1-2B_1+6A_2+6B_2+8B_3,$$
$$m\omega_{\mathrm{TO\parallel(TA\parallel)}}{}^2=8a_1+2a_3+6b_3+8A_1+4A_3+12B_3,$$
$$m\omega_{\mathrm{TA\parallel(TO\parallel)}}{}^2=8a_1+2a_3+6b_3-2A_1+6B_1+6A_2+6B_2+8A_3.$$

There is no *a priori* way of deciding which expression should refer to the $m\omega^2(\mathrm{LA})$ at M or which to the $m\omega^2(\mathrm{LO})$, since they are obtained as

$$(8b_1+6a_3+2b_3+3A_1+3B_1+3A_2+3B_2+6A_3+6B_3)\pm|3A_1-5B_1+3A_2+3B_2-6A_3+2B_3|,$$

and similarly for $m\omega^2(\mathrm{TA}\parallel)$ and $m\omega^2(\mathrm{TO}\parallel)$ at M. We have found the order of the expressions given above (where the expression refers to the modes listed outside parentheses) to be consistent with our data.

Finally, the rotational invariance condition is given as

$$(\gamma^2/4)[4a_2+4b_2+3(A_1+B_1+A_2+B_2+2A_3+2B_3)]=3g_1+9g_3+G_1+4G_2+14G_3.$$